



**University of
Zurich** UZH

**Zurich Open Repository and
Archive**

University of Zurich
University Library
Strickhofstrasse 39
CH-8057 Zurich
www.zora.uzh.ch

Year: 2014

Mechanisms of Water Interaction with Pore Systems of Hydrochar and Pyrochar from Poplar Forestry Waste

Conte, Pellegrino ; Hanke, Ulrich Michael ; Marsala, Valentina ; Cimò, Giulia ; Alonzo, Giuseppe ; Glaser, Bruno

DOI: <https://doi.org/10.1021/jf5010034>

Posted at the Zurich Open Repository and Archive, University of Zurich

ZORA URL: <https://doi.org/10.5167/uzh-97236>

Journal Article

Accepted Version

Originally published at:

Conte, Pellegrino; Hanke, Ulrich Michael; Marsala, Valentina; Cimò, Giulia; Alonzo, Giuseppe; Glaser, Bruno (2014). Mechanisms of Water Interaction with Pore Systems of Hydrochar and Pyrochar from Poplar Forestry Waste. *Journal of agricultural and food chemistry*, 62(21):4917-4923.

DOI: <https://doi.org/10.1021/jf5010034>

MECHANISMS OF WATER INTERACTION WITH PORE SYSTEMS OF HYDROCHAR AND PYROCHAR FROM POPLAR FORESTRY WASTE

Pellegrino Conte, Ulrich M. Hanke, Valentina Marsala, Giulia Cimò, Giuseppe Alonzo, and Bruno Glaser

J. Agric. Food Chem., **Just Accepted Manuscript** • Publication Date (Web): 09 May 2014

Downloaded from <http://pubs.acs.org> on May 11, 2014

Just Accepted

“Just Accepted” manuscripts have been peer-reviewed and accepted for publication. They are posted online prior to technical editing, formatting for publication and author proofing. The American Chemical Society provides “Just Accepted” as a free service to the research community to expedite the dissemination of scientific material as soon as possible after acceptance. “Just Accepted” manuscripts appear in full in PDF format accompanied by an HTML abstract. “Just Accepted” manuscripts have been fully peer reviewed, but should not be considered the official version of record. They are accessible to all readers and citable by the Digital Object Identifier (DOI®). “Just Accepted” is an optional service offered to authors. Therefore, the “Just Accepted” Web site may not include all articles that will be published in the journal. After a manuscript is technically edited and formatted, it will be removed from the “Just Accepted” Web site and published as an ASAP article. Note that technical editing may introduce minor changes to the manuscript text and/or graphics which could affect content, and all legal disclaimers and ethical guidelines that apply to the journal pertain. ACS cannot be held responsible for errors or consequences arising from the use of information contained in these “Just Accepted” manuscripts.



1 **MECHANISMS OF WATER INTERACTION WITH PORE SYSTEMS OF HYDROCHAR**
2 **AND PYROCHAR FROM POPLAR FORESTRY WASTE**

3 Pellegrino Conte^{1*}, Ulrich M. Hanke^{2,†}, Valentina Marsala¹, Giulia Cimò¹, Giuseppe Alonzo¹,
4 Bruno Glaser²

5 1. Dipartimento di Scienze Agrarie e Forestali, Università degli Studi di Palermo v.le delle
6 Scienze edificio 4, 90128 Palermo – Italy

7 2. Soil Biogeochemistry, Martin-Luther-University Halle-Wittenberg, von-Seckendorff-Platz
8 3, 06120 Halle – Germany

9

10

11 **Running title:** Water dynamics on hydrochar and pyrochar surfaces

12

13

14

15 ***. Corresponding and contact author:** Pellegrino Conte; E-Mail: pellegrino.conte@unipa.it; Ph.:

16 003909123864673; Fax: 0039091484035

17

18 [†]. Present address: Soil Science and Biogeochemistry, University of Zurich, Winterthurerstrasse

19 190, 8057 Zürich - Switzerland

20

21 **Abstract**

22 The aim of this paper was to understand the water-surface interactions of two chars obtained by
23 gasification (pyrochar) and hydrothermal carbonization (hydrochar) of a poplar biomass. The two
24 samples revealed different chemical composition as evidenced by solid state ^{13}C NMR
25 spectroscopy. In fact, hydrochar resulted in a lignin-like material still containing oxygenated
26 functionalities. Pyrochar was a polyaromatic system where no hetero-nuclei were detected. After
27 saturating with water, hydrochar and pyrochar were analyzed by fast field cycling (FFC) NMR
28 relaxometry. Results showed that water movement in hydrochar was mainly confined in very small
29 pores. Conversely, water movement in pyrochar led to the conclusion that a larger number of
30 transitional and very large pores were present. These results were confirmed by porosity evaluation
31 derived from gas adsorption. Variable temperature FFC NMR experiments confirmed slow motion
32 regime due to a preferential diffusion of water on the solid surface. Conversely, the larger number
33 of large pores in pyrochar allowed slow movement only up to 50 °C. As temperature was raised to
34 80 °C, water interactions with the pore surface became weaker, thereby allowing a 3D water
35 exchange with the bulk liquid. This paper has shown that pore size distribution was more important
36 than chemical composition in affecting water movement in two chemically different charred
37 systems.

38

39 **Keywords:** fast field cycling NMR; relaxometry; hydrochar; pyrochar; biochar; water dynamics

40 Introduction

41 Recent scientific research addressed applications of charred biomasses for environmental
42 remediation and agricultural productivity.¹⁻³ In fact, use of charred biomasses has been suggested as
43 a solution to counteract enhancement of atmospheric carbon dioxide,^{4,5} for water and soil
44 remediation⁶⁻⁸ and for improvement of soil fertility.² In particular, char applied deliberately to soils,
45 which Lehmann and Joseph⁹ have recently classified as biochar, can modify soil pH,¹⁰ increase soil
46 draining capacity,¹¹ improve cation exchange capacity,¹² mitigate salt-induced stresses¹³ and
47 interact with soil fertilizers,¹⁴ thereby favoring microbial activity¹⁵ and plant growth.^{14,16}

48 Notwithstanding the positive effects of biochar applications to soils, some authors have warned
49 about its potential detrimental impacts on environment. For example, increase of CO₂ emissions to
50 atmosphere, due to enhancement of soil C mineralization rate after biochar applications to soils, has
51 been described.¹⁷ Also plant growth inhibition due to temporary high pH values, presence of volatile
52 matter (i.e. tars, resins, and other short-lived substances that remain on the biochar surface
53 immediately after production), and nutrient imbalances associated with the use of fresh biochars
54 have been reported.^{18,19}

55 Certainly, functions of chars in the environment depend on their physico-chemical properties which,
56 in turn, are most affected by feedstock type, pyrolysis conditions, and duration of charring.^{3,9-11,20-25}

57 As an example, aromatic condensation in chars increases with increasing heating temperature.^{20,24}

58 Moreover, plant species with many large diameter cells in the stem tissues can lead towards chars
59 containing larger amounts of macro pores.⁹ Macro pores in biochar applied to soils may enhance
60 soil draining properties and capacity to retain large molecules such as phenolic compounds.¹¹ On
61 the other hand, micro pores may adsorb water with high capillary forces so that it is not available
62 for most plants. For this reason, understanding char physical and chemical processes at the char
63 surface is very crucial in order to address its agronomical and environmental uses and allow
64 meaningful pre-application quality assessments.

65 Nuclear magnetic resonance (NMR) techniques are usually applied to monitor char
66 characteristics.^{10,20,22,24,26} In particular, low field NMR relaxometry with fast field cycling setup
67 (FFC NMR) can be used to study the dynamics of water in chars in order to retrieve information
68 about the possible molecular mechanisms through which water (and therefore micro and macro
69 nutrients) can be drained in char-amended soils.

70 In previous studies, FFC NMR relaxometry was applied to differentiate among pore size
71 distribution on the surface of chars obtained by an industrial gasification procedure¹⁰ and to
72 recognize the nature of the interactions between water and char surfaces.²⁶ These studies were
73 conducted only on chemically identical chars. However, no information is available on the
74 dynamics of water in chars having different chemical composition. For this reason, in the present
75 study, we selected a hydrochar already analyzed by Wiedner et al.²⁴ and a pyrochar studied in De
76 Pasquale et al.¹⁰ and Conte et al.²⁶, both obtained by the same biomass feedstock, with the aim to
77 investigate the role played by chemical characteristics on water dynamics within the pore system of
78 the chars.

79

80 **Materials and Methods**

81 **Feedstock.** The hydrochar and pyrochar samples were prepared by using poplar (*Populus spp.* L.)
82 wood chips which were obtained from dedicated short rotation forest in the Po Valley (Gadesco
83 Pieve Delmona, 45°10'13" N, 10°06'01" E). The age of the forest at the time of harvest was five
84 years. The characteristics of the biomass were already described in De Pasquale et al.¹⁰

85 **Pyrochar and hydrochar preparation.** Pyrochar was produced by using an industrial gasifier at
86 the temperature of 1200 °C. All the details about the gasifier and the pyrolytic conditions have been
87 already reported in De Pasquale et al.¹⁰ Hydrochar was obtained in a b.coal 2.0 reactor from Artec
88 Biotechnology GmbH (Bad Königshofen, Germany) at 230 °C and 40 bar. Details about the
89 procedure have been reported already in Wiedner et al.²⁴ Both pyrochar and hydrochar samples

90 were 2 mm sieved with a stainless steel sieve and dried overnight in an oven set at 105 °C before
91 each NMR analysis.

92 **Specific surface area measurement.** Samples were first dried at 200 °C for 4.5 hours, then stored
93 in a desiccator. In order to retrieve the specific surface area by applying the Brunauer–Emmett–
94 Teller (BET) 5-points method, samples were degassed with N₂ at 200 °C for another hour and then
95 measured in liquid N₂ (Quantachrome NOVA 4200 calibrated with BAM-PM-104) following DIN
96 ISO 9277:2003-05. All measurements were done in triplicate. Specific surface area of the pyrochar
97 and the hydrochars were $54.6 \pm 0.2 \text{ m}^2\text{g}^{-1}$ and $129 \pm 2 \text{ m}^2\text{g}^{-1}$, respectively.

98 The poplar pyrochar surface area measured in this study was smaller than that already reported in
99 De Pasquale et al.¹⁰ (i.e. $98 \pm 6 \text{ m}^2\text{g}^{-1}$). The difference can be explained by the different sample
100 preparation used in De Pasquale et al.¹⁰ prior to BET analysis. In fact, the BET investigations
101 reported in De Pasquale et al.¹⁰ have been conducted on agate-mortar-ground samples. Pyrochar
102 grinding reduces particle sizes, thereby increasing surface area values.

103 **Evaluation of pore size distribution from the specific surface area measurements.** The non-
104 local density functional theory (NLDFT) equilibration model²⁷ was applied to elaborate the
105 isotherms (35 adsorption and 30 desorption points) of nitrogen adsorption experiments in order to
106 achieve pore size distributions. Assumption of N₂ at -196 °C on carbon (slit-pore) was used. The
107 cumulative pore volumes and surface areas for the micro pore class (i.e. < 2 nm, according to
108 IUPAC classification) retrieved by NLDFT model were $16.3 \times 10^{-3} \text{ cm}^3\text{g}^{-1}$ and $29.4 \text{ m}^2\text{g}^{-1}$ for
109 pyrochar, while they resulted $50.9 \times 10^{-3} \text{ cm}^3\text{g}^{-1}$ and $93.3 \text{ m}^2\text{g}^{-1}$ for hydrochar. NLDFT surface area
110 and pore volume for hydrochar resulted around three times higher than those for pyrochar, thereby
111 evidencing that the amount of pores in the former sample was larger than in the latter one. In
112 particular the Surface/Volume (S/V) ratios from NLDFT elaborations were $(S/V)_{\text{pyrochar}} = 1.80 \times 10^9$
113 m^{-1} and $(S/V)_{\text{hydrochar}} = 1.83 \times 10^9 \text{ m}^{-1}$.

114 **CP-TOSS ¹³C NMR spectra.** Cross polarization magic angle spinning (CPMAS) ¹³C NMR
115 measurements were performed on a Bruker Avance-II 400 spectrometer (Bruker Biospin, Milan,

116 Italy) operating at 100.6 MHz on carbon-13 and equipped with a 4 mm standard bore solid state
117 probe. Samples were packed into 4 mm zirconia rotors with Kel-F caps and the rotor spin rate was
118 set at 5000 ± 2 Hz. A spectral width of 25252.52 Hz centered at 10061.78 Hz, an optimum contact
119 time of 1 ms chosen after evaluation of variable contact time experiments, a recycle delay of 20 s, 2
120 k data points over an acquisition time of 35 ms were used. The spectra were acquired with the total
121 suppression side bands (TOSS) sequence with a 50% RAMP in order to prevent artifacts in the
122 spectra interpretation. A $4.1 \mu\text{s}$ ^1H 90° pulse with an attenuation level of -2.4 dB was applied.
123 Spectra acquisition was achieved with Bruker Topspin[®] 2.0. Data processing was done with
124 MestRe-C software (Version 4.9.9.9, Mestrelab Research, Santiago de Compostela, Spain). The free
125 induction decays (FIDs) were transformed by applying first a 2 k zero filling, then a line broadening
126 of 100 Hz and finally an automatic baseline correction with a 3rd order polynomial and Bernstein
127 algorithm.

128 **Fast field cycling (FFC) NMR relaxometry.** The 2 mm sieved and dried poplar pyrochar and
129 hydrochar samples have been prepared as slurry for fast field cycling (FFC) NMR relaxometry
130 investigations according to the procedure reported in Dunn et al.²⁸ The background theory of FFC
131 NMR relaxometry has been already described in De Pasquale et al.¹⁰ Moreover, more general
132 environmental applications of FFC NMR relaxometry can be found in Conte and Alonzo.²⁹
133 ^1H nuclear magnetic resonance dispersion profiles (i.e. relaxation rates R_1 or $1/T_1$ vs. proton Larmor
134 frequencies) were acquired on a Stellar Spinmaster FFC2000 Relaxometer (Stelar s.r.l., Mede, PV–
135 Italy) at temperatures of 25 °C, 50 °C and 80 °C. The proton spins were polarized at a B_{POL}
136 corresponding to the proton Larmor frequency (ω_L) of 24 MHz for a T_{POL} corresponding to about
137 five times the T_1 estimated at this frequency. After each B_{POL} application, the magnetic field
138 intensity (indicated as B_{RLX}) was systematically changed in the proton Larmor frequency ω_L
139 comprised in the range 0.01-40 MHz. The period τ , during which B_{RLX} was applied, has been varied
140 on 32 logarithmic spaced time sets, each of them adjusted at every relaxation field in order to

141 optimize the sampling of the decay/recovery curves. Free induction decays (FID) were recorded
142 following a single ^1H 90° pulse applied at B_{ACQ} corresponding to the proton Larmor frequency of
143 16 MHz. A time domain of 100 μs sampled with 512 points was applied. Field switching time was
144 3 ms, while spectrometer dead time was 15 μs . For all experiments, a recycle delay of 12 s was
145 used. The NP sequence was applied when the relaxation magnetic fields were in the range of the
146 proton Larmor frequencies between 40.0 and 9.0 MHz. The PP sequence was applied in the proton
147 Larmor frequencies B_{RLX} range of 9.0-0.01 MHz.³⁰

148 **FFC NMR data processing.** R_1 values were achieved by interpolating the ^1H magnetization
149 decay/recovery curves at each B_{RLX} value (i.e. ^1H signal intensity versus τ) with the stretched
150 exponential function (also known as Kohlrausch-Williams-Watts function) reported in equation [1]
151 after exportation of the experimental data to OriginPro 7.5 SR6 (Version 7.5885, OriginLab
152 Corporation, Northampton, MA, USA). This equation provided the best fitting with the largest
153 coefficients of determination ($R^2 > 0.998$). The choice of this function was due to the large sample
154 heterogeneity resulting in a multi-exponential behavior of the decay/recovery curves.^{29,31} This
155 approach has the advantage that it is able to handle a wide range of behaviors within a single model.
156 For this reason, assumptions about the number of exponentials to be used in modeling NMRD data
157 are not necessary.

$$158 \quad I(\tau) = I_0 \exp\left[-(\tau/T_1)^k\right] \quad [1].$$

159 In equation [1], $I(\tau)$ is the ^1H signal intensity at each fixed B_{RLX} , I_0 is the ^1H signal intensity at the
160 thermal equilibrium, T_1 is the average proton spin lattice relaxation time and k is a heterogeneity
161 parameter related to the stretching of the decay process. This function can be considered as a
162 superposition of exponential contributions, thereby describing the likely physical picture of some
163 distribution in T_1 .

164 Relaxation data at the proton Larmor frequency of 40 MHz were evaluated by the inverse Laplace
165 transformation through application of the UPEN algorithm (Alma Mater Studiorum – Università di

166 Bologna, Italy)^{32,33} with the aim to obtain the T_1 distributions at such magnetic field and, therefore,
167 information on pore distribution, and grain size. The choice of UPEN analyses only at 40 MHz was
168 due to the larger NMR sensitivity at this frequency as compared to the other proton Larmor
169 frequencies.³⁰

170

171 **Results and Discussion**

172 **Hydrochar and pyrochar chemical composition by CP-TOSS ^{13}C NMR spectroscopy.** The
173 cross polarization magic angle spinning with total suppression of side bands ^{13}C NMR spectra of
174 the two samples studied here, showed the more complex nature of hydrochar as compared to
175 pyrochar (Figure 1). In particular, two main regions can be recognized in the hydrochar spectrum
176 (Figure 1A). The first chemical shift interval between 0 – 80 ppm contains individual signals at 16,
177 30, 48, 56 and 72 ppm (Figure 1A). The first signal at 16 ppm can be attributed to methyl groups of
178 terminating alkyl chains; the second one at 30 ppm is due to methylene groups in alkyl chains,
179 whereas the signal at 48 ppm can be assigned to branched alkyl carbons; the signal at 56 ppm is
180 assignable to methoxyl groups in lignin-like structures and that at 72 ppm is due to carbons C2, C3,
181 C5 in the residual cellulose moiety from the poplar biomass.^{24,34}

182 The second spectral region in Figure 1A occurred in the chemical shift interval between 90 – 160
183 ppm. The main signals recognized in this region are broad bands centered at 106, 115, 133 and 147
184 ppm. The signal at 106 ppm can be assigned to C1 in residual cellulose; that at 115 ppm is due to
185 C5 in guaiacyl (G) and C3 and C6 in *p*-hydroxyphenyl groups; the signal at 133 ppm is due to the
186 aromatic C–5/C–5' in etherified 5–5 G units; finally the signal at 147 ppm is assigned to C3 and C4
187 in etherified guaiacyl units.^{24,34}

188 The spectrum reported in Figure 1B reveals only one broad band at 126 ppm which can be assigned
189 to polyaromatic systems.¹⁰ The differences in the chemical composition of poplar hydrochar and
190 pyrochar samples (Figure 1) can be explained by the different types of reactions occurring as either
191 hydrothermal carbonization²⁴ or gasification¹⁰ are applied. The hydrothermal carbonization used in

192 this study consisted of a thermal degradation of the water-suspended-biomass at high pressure and
193 230 °C by applying citric acid as catalyst.²⁴ During this process, carbohydrates in poplar biomass
194 have been gradually transformed to aromatic and aliphatic structures, thereby providing a lignin-
195 like material. However, the presence of signals at 56, 72, 106, 133 and 147 ppm (Figure 1A)
196 indicates that the hydrothermal carbonization produced a carbonaceous material still containing
197 oxygenated functionalities, but almost no poly-condensed aromatic moieties as outlined in Wiedner
198 et al.²⁴

199 The sole aromatic signal in the CP-TOSS ¹³C NMR spectrum of the poplar pyrochar (Figure 1B) is
200 due to the diamagnetic currents produced by delocalized π -electrons in extended aromatic structures
201 or graphite-like micro-crystallites which are generated by the high temperature condensations as
202 biomass feedstock is subjected to gasification.¹⁰

203 **Effect of pore size on ¹H NMR T₁ distributions.** The 2 mm sieved poplar hydrochar and pyrochar
204 samples were saturated with water and the slurry analyzed by fast field cycling NMR relaxometry
205 as indicated in Materials and Methods. Figure 2 reports the distributions of the longitudinal
206 relaxation times (T₁), also referred to as relaxograms, at the proton Larmor frequency of 40 MHz
207 and three temperatures (25, 50 and 80 °C) as obtained by applying the inverse Laplace
208 transformation of the relaxation data through the UPEN algorithm (see Materials and Methods).

209 Proton longitudinal relaxation times of water in porous media are affected by the collisions between
210 the liquid state molecules and the walls of the porous boundaries.³⁵ In particular, longitudinal
211 relaxation is dominated by the presence of a strong relaxation sink at the pore surface which is
212 imputable to the temporary adsorption of water on the solid surface.³⁶ Temporary adsorption can be
213 achieved by formation of weak un-conventional hydrogen bonds on the surface of pyrogenic char
214 systems as already outlined in Conte et al.²⁶ and Conte and Alonzo.²⁹ However, as surficial polar
215 groups are present, the weak un-conventional H-bonds may turn towards stronger conventional ones
216 which may hook water molecules more strongly on the char surface. The effectiveness of the
217 aforementioned relaxation sink depends on the ratio between the pore surface and the pore volume

218 as well as on the diffusion rate across the pore.³⁷ In fact, space restriction in small sized pores do
219 not allow fast molecular mobility. As this condition occurs, ^1H - ^1H dipolar interactions result very
220 efficient. Shorter relaxation times are, hence, retrieved.^{35,37,38} Conversely, as pore size enlarges,
221 molecular mobility increases and strength of dipolar interactions weaken. For this reason, longer
222 relaxation times are expected.^{35,37,38} As the number and size of the various pores present in a
223 material is heterogeneous, water must diffuse through the differently sized pores, thereby providing
224 a wide ensemble of longitudinal relaxation times which appear continuously distributed. The lowest
225 limit of such ensemble (the shortest T_1 value) is due to water moving into the smallest pores,
226 whereas the highest limit (the longest T_1 value) is attributed to water moving into the largest pores.
227 All T_1 values between the two limits are due to the dynamics of water inside pores having sizes
228 lying between the two extremes.²⁹ According to the aforementioned mechanism, the differences
229 observed at the same temperatures between the T_1 distributions reported in Figure 2 can be
230 attributed to different pore size distribution present in the hydrochar and pyrochar samples. In
231 particular, a homogeneous distribution of small sized pores can be recognized in hydrochar rather in
232 pyrochar. The latter, in turn, is made by a less homogeneous distribution of pores which are
233 averagely larger than in hydrochar. In fact, all the hydrochar relaxograms showed a maximum
234 centered at a T_1 value of around 100 ms regardless of the temperature used during the experiments
235 (Figure 2A). Conversely, the relaxograms acquired for the water-saturated pyrochar span a larger
236 interval of T_1 values (Figure 2B). Here a maximum at 100 ms independent of the applied
237 temperature (similarly to the water-saturated hydrochar sample) can be observed. Moreover, a
238 second maximum centered at 479, 340 and 290 ms retrieved at 25 °C, 50 °C and 80 °C,
239 respectively, is also observed (Figure 2B). A wide distribution of T_1 values is included among the
240 two longitudinal relaxation time limits in Figure 2B. We can identify water molecules relaxing at
241 100 ms in both carbonaceous samples as those restricted in the smallest sized pores; water
242 molecules generating the maxima at 479 ms at 25 °C, 340 ms at 50 °C and 290 ms at 80 °C as those

243 tumbling in the largest pores; finally, water molecules relaxing in the intervals 100 – 479 ms at 25
244 °C, 100 – 340 ms at 50 °C and 100 – 290 ms at 80 °C as those occluded in transitional pores.

245 The aforementioned findings are supported by BET and NLDFT elaborations as reported in
246 Materials and Methods. In fact, specific surface areas were $54.6 \pm 0.2 \text{ m}^2\text{g}^{-1}$ and $129 \pm 2 \text{ m}^2\text{g}^{-1}$ for
247 pyrochar and hydrochar respectively, thereby suggesting a larger volume of pores in the former than
248 in the latter sample. On the other hand, NLDFT elaborations of isotherms obtained from nitrogen
249 adsorption provided S/V ratios in the order $(S/V)_{\text{pyrochar}} < (S/V)_{\text{hydrochar}}$ (see Material and Methods).

250 It is well known that the longitudinal relaxation rate ($1/T_1$) is directly proportional to the S/V ratio³⁹
251 or, by considering the reciprocal:

$$252 \quad T_1 \propto \frac{V}{S}$$

253 Since $(S/V)_{\text{pyrochar}} < (S/V)_{\text{hydrochar}}$, it comes that $(V/S)_{\text{pyrochar}} > (V/S)_{\text{hydrochar}}$ and it is expected that the
254 T_1 values for pyrochar must be longer than for hydrochar. The latter expectation has been evidenced
255 in the experimental results showed in Figure 2 and discussed above.

256 It is interesting to note that the relaxogram reported in De Pasquale et al.¹⁰ was obtained for the
257 same pyrochar used in the present study. However, the T_1 distribution in De Pasquale et al.¹⁰
258 revealed a larger pore size homogeneity than the relaxogram reported here in Figure 2B. This
259 difference can be explained by considering that samples were prepared differently prior to the
260 analysis. In fact, in the present study, we sieved the poplar pyrochar $< 2 \text{ mm}$, whereas in De
261 Pasquale et al.¹⁰ the sample has been grounded. As already outlined in Materials and Methods,
262 sample grinding reduces pore size, thereby allowing larger surface area and more homogeneous
263 pore size distribution.

264 **Effect of temperature on ^1H NMR T_1 distributions.** Longitudinal relaxation times are not only
265 dependent on the pore size distribution, as outlined in the previous paragraph, but also on
266 temperature variations.²⁹ In fact, it is well recognized that temperature increments accelerate
267 molecular motions, thereby weakening the ^1H - ^1H dipolar interactions responsible for the

268 longitudinal relaxation of a liquid moving on the surface of porous materials.⁴⁰ When this condition
269 occurs, an increase of T_1 values is expected since a longer time is needed for proton spin lattice
270 relaxation. However, it has been already shown that water retained in charred materials behaves
271 diametrically, thereby suggesting that water dynamics is subjected to a slow motion regime.²⁶ The
272 latter is achieved when water molecules are hooked to the char surface via weak hydrogen bonds
273 that may arise by the overlay of the electron-deficient orbitals of protons in water and the electron-
274 rich orbitals in the organic and inorganic components of the charred system.²⁶ As temperature
275 increases, the weak interactions, which allow water adhesion to the pore walls, oppose to the 3D
276 exchange with the bulk water (i.e. the replacement of water molecules hooked to the char surface
277 with those appertaining to the bulk liquid).⁴⁰ For this reason, water preferentially diffuses faster
278 within the channels connecting pores between each other through a 2D motion (i.e. the diffusion of
279 water molecules within the channels connecting either different surface pores or char surface with
280 the interior part of the same material).^{26,40} Due to the 2D surface diffusion just described, water
281 collision frequency with pore walls increases with temperature, thereby allowing an average
282 residence time on pore walls longer than that retrieved at lower temperatures. Because of this,
283 shorter time for protons to relax is needed and lower T_1 values are achieved.⁴⁰ As a consequence,
284 relaxograms, such as those in Figure 2, shrink as temperature is increased. Moreover, it must be
285 added that the larger the pore size, the more pronounced is the reduction of the relaxogram width
286 and the reduction of the T_1 maxima. In fact, upon temperature increasing, water collision frequency
287 in larger pores becomes higher than in the more spatially restricted ones. Because of this, the
288 average time spent by water molecules on pore walls is higher in the transitional and the largest
289 pores than in the smallest pores. The latter is the reason why the reduction of relaxogram widths is
290 less pronounced in Figure 2A than in Figure 2B. Moreover, the same mechanism explains why the
291 maximum at 100 ms due to water in the smallest pores either in hydrochar or in pyrochar is
292 unaffected by temperature changes, whereas the T_1 maxima due to water in larger sized pores (T_1
293 >100 ms) shift towards shorter values.

294 **NMRD profiles.** Figure 3 shows the nuclear magnetic resonance dispersion (NMRD) profiles (i.e.
295 $R_1=1/T_1$ values vs ω_L) at 25, 50 and 80 °C for the water-saturated poplar hydrochar and pyrochar
296 samples investigated here. In particular, the NMRD profiles of the former sample are all placed at
297 faster longitudinal relaxation rates (Figure 3A) as compared to the NMRD profiles of the latter
298 sample (Figure 3B). This is due to the differences in the surface areas between the two porous
299 materials. In fact, $SSA_{\text{hydrochar}}$ was larger than SSA_{pyrochar} (see above). The larger the surface area
300 value, the smaller is the size of the pores. Restriction of water in small pores leads to stronger ^1H - ^1H
301 dipolar interactions which, in turn, are the cause for the very efficient proton longitudinal relaxation
302 in hydrochar (i.e. faster R_1 values) compared to pyrochar.⁴¹

303 It is worth to note that all the NMRD profiles in Figure 3A are translated towards faster R_1 values in
304 the whole range of proton Larmor frequencies as temperature was increased. This behavior accords
305 with that already described in Conte et al.²⁶, thereby confirming the slow motion regime also
306 outlined in the previous paragraph. However, Conte et al.²⁶ reported that the slow motion regime on
307 the surface of char systems is due to non-conventional H-bonds arising by the overlay between the
308 electron-deficient orbitals of protons in water and the electron-rich orbitals of the aromatic organic
309 centers in the charred material. In the present study, we have reported that hydrothermal
310 degradation did not remove all the oxygen-containing functionalities (see above). For this reason,
311 we cannot exclude participation of the more traditional O-H \cdots O bonds in the slow motion regime
312 observed for the hydrochar sample.

313 Figure 3B reveals that the NMRD profiles acquired for the pyrochar sample behaved similarly to
314 the hydrochar only up to 50 °C. Conversely, an anomalous trend was observed at 80 °C. In fact, a
315 slight increment of the R_1 values was retrieved between 40 and 10 MHz as temperature was
316 switched from 50 to 80 °C. Then the 80 °C NMRD profile crossed the one acquired at 50 °C as ω_L
317 was set to 10 MHz and that retrieved at 25 °C as ω_L was switched to 0.2 MHz (Figure 4B). The H-
318 bond-mediated slow motion regime can explain the NMRD behavior up to 50 °C observed for the

319 pyrochar sample (Figure 3B). However, as temperature is raised up to 80 °C, a chemical exchange
320 with the bulk phase must be considered in order to account for the anomalous behavior reported in
321 Figure 3B.⁴⁰

322 The interesting feature that the temperature dependence of water dynamics in hydrochar is opposite
323 to that observed in pyrochar can only be explained by considering the different pore size
324 distribution in the two carbonaceous samples. In fact, as outlined above, the average pore size in
325 hydrochar is smaller than in pyrochar. Water molecules are more tightly trapped in the former than
326 in the latter material. For this reason, water can easily run away towards the bulk liquid from
327 pyrochar rather than from hydrochar surface as temperature was increased up to 80 °C.

328 The comparison among the temperature dependence of the NMRD profiles in Figure 3 and those in
329 Conte et al.²⁶ supports the latter hypothesis on the role played by pore size in water exchange with
330 the bulk solution. In fact, the pyrochar analyzed either in the present study or in Conte et al.²⁶ was
331 obtained by the same gasification process.¹⁰ However, while in Conte et al.²⁶ the pyrochar was
332 grounded in an agate mortar before NMRD investigations, here we have performed NMRD
333 analyses after having sieved the same material < 2 mm. As a consequence, the surface area of the
334 grounded pyrochar²⁶ resulted larger than that used in the present study. As already noted above,
335 larger surface area was associated with a more homogeneous pore size distribution made mainly by
336 the smallest pores. Conversely, more inhomogeneous distribution of pore size (with a larger
337 contribution from transitional and larger pores) was identified in the porous charred material having
338 lower surface area. Hence, the more inhomogeneous pore size pyrochar used here revealed the
339 anomalous temperature dependence behavior at 80 °C (Figure 3B) due to the higher amount of
340 larger pores which make the exchange of surface water molecules with the bulk ones easier.

341 This paper reports about high and low field NMR characterization of the physico-chemical
342 properties of hydrochar and pyrochar samples retrieved by applying either hydrothermal treatment
343 or gasification to poplar forestry wastes. In particular, high field NMR spectroscopy (i.e. CP-TOSS
344 ¹³C NMR) revealed that the thermal treatments produced two chemically different carbonaceous

345 materials. While poplar hydrochar appeared as a lignin-like material still containing oxygenated
346 functionalities, poplar pyrochar emerged as a polyaromatic system where O-containing groups were
347 not detected.

348 Notwithstanding the different chemical compositions, the mechanisms of water dynamics on the
349 surface of poplar hydrochar and pyrochar were affected more by their physical characteristics rather
350 than by their chemical peculiarities. In particular, isothermally 40 MHz acquired relaxograms
351 revealed that water motion was more restricted in hydrochar than in pyrochar, thereby suggesting
352 that the former sample included a larger number of small-sized pores than the latter one. On the
353 other hand, the more free motion of water in pyrochar indicated a higher amount of transitional and
354 very large pores.

355 Variable temperature relaxometry experiments revealed that 2D surface diffusion mechanism was
356 the only force responsible for water motion in hydrochar up to the temperature of 80 °C. Surface
357 diffusion was the predominating motion mechanism of water in pyrochar only up to 50 °C.
358 Conversely, a 3D exchange with the bulk water appeared to interfere with the aforementioned 2D
359 diffusion as temperature was raised up to 80 °C.

360 The differentiation between the 2D diffusion and the 3D exchange mechanisms was attributed to the
361 different porosity in the charred materials. In fact, water constrained in small pores such as in
362 hydrochar strongly interacts with the solid surfaces. For this reason, its fugacity towards the bulk
363 liquid is inhibited in the whole temperature interval investigated here (25 – 80 °C). On the other
364 hand, the larger pore sizes in poplar pyrochar prevent water exchange with the bulk solution only in
365 a more restricted temperature interval (namely, 25 – 50 °C). As temperature overcomes the limit of
366 50 °C, water surface interactions become weaker and 3D exchange with the bulk liquid occurs.

367 Although in the present study the chemical composition of poplar hydrochar and pyrochar appeared
368 of minor importance to the water dynamics, its contribution to the strength of water solid phase
369 interactions is not yet clear. For this reason, more detailed studies on the effect of pore sizes and
370 chemical composition of charred materials on water dynamics are urgently needed.

371 **Acknowledgments**

372 The authors are grateful to Centro Grandi Apparecchiature – UniNetLab of Università degli Studi di
373 Palermo (<http://www.unipa.it/cga/index.html>) for having provided machine time at the high field
374 NMR spectrometer for the acquisition of the CP-TOSS ^{13}C NMR spectra.

375 We appreciate the support of COST action TD1107 (Biochar for sustainable resources
376 management) for the Short-term Scientific Mission (STSM) of Ulrich M. Hanke.

377 Dr. Alessandro Pozzi (AGT technologies) is acknowledged for providing the pyrochar sample.

378

379 **References**

- 380 1. Glaser, B.; Haumaier, L.; Guggenberger, G.; Zech, W. The “Terra Petra” phenomenon a
381 model for sustainable agriculture in the humid tropics. *Naturwissenschaften* **2001**, *88* (1),
382 37-41; DOI: 10.1007/s001140000193.
- 383 2. Mao, J. D.; Johnson, R. L.; Lehmann, J.; Olk, D. C.; Neves E. G.; Thomson M. L.; Schmidt-
384 Rohr, K. Abundant and stable char residues in soils: implication for soil fertility and carbon
385 sequestration. *Environ. Sci. Technol.* **2012**, *46*, 9571-9576.
- 386 3. Mukherjee, A.; Lal, R. Biochar impacts on soil physical properties and greenhouse gas
387 emissions. *Agron.* **2013**, *3* (2), 313-339; DOI: 10.3390/agronomy3020313.
- 388 4. Glaser, B.; Lehmann, J.; Zech, W. Ameliorating physical and chemical properties of highly
389 weathered soils in the tropics with charcoal – a review. *Biol. Fert. Soils* **2002**, *35* (4), 219-
390 230; DOI: 10.1007/s00374-002-0466-4.
- 391 5. Vanderslice, N. C.; Marrero, T. R. Impact of Bio-Char on Carbon Dioxide in the
392 Atmosphere. In *Proceedings of the 2009 Midwest Section Conference of the American*
393 *Society for Engineering Education*; available at: [http://www.asee.org/papers-and-](http://www.asee.org/papers-and-publications/papers/section-proceedings/midwest/2009)
394 [publications/papers/section-proceedings/midwest/2009](http://www.asee.org/papers-and-publications/papers/section-proceedings/midwest/2009)

- 395 6. Mohan, D.; Rajput, S.; Singh, V. K.; Steele, P. H.; Pittman Jr., C. U. Modeling and
396 evaluation of chromium remediation from water using low cost bio-char, a green adsorbent.
397 *J. Hazard. Mater.* **2011**, *188* (1-3), 319–333; DOI: 10.1016/j.jhazmat.2011.01.127.
- 398 7. Beesley L.; Moreno-Jiménez E.; Gomez-Eyles J. L.; Harris E.; Robinson B.; Sizmur T. A
399 review of biochars' potential role in the remediation, revegetation and restoration of
400 contaminated soils. *Environ. Pollut.* **2011**, *159* (12), 3269–3282; DOI:
401 10.1016/j.envpol.2011.07.023.
- 402 8. Zhang, X.; Wang, H.; He, L.; Lu, K.; Sarmah, A.; Li, J.; Bolan, N. S.; Pei, J.; Huang, H.
403 Using biochar for remediation of soils contaminated with heavy metals and organic
404 pollutants. *Environ. Sci. Pollut. R.* **2013**, *20* (12); DOI 10.1007/s11356-013-1659-0.
- 405 9. Lehmann, J.; Joseph, S. Biochar for environmental management: an introduction. In *Biochar*
406 *for environmental management: science and technology*; Lehmann, J.; Joseph, S.; Eds.;
407 Routledge: London U. K. 2009; pp. 448.
- 408 10. De Pasquale, C.; Marsala, V.; Berns, A.E.; Valagussa, M.; Pozzi, A.; Alonzo, G.; Conte, P.
409 Fast field cycling NMR relaxometry characterization of biochars obtained from an industrial
410 thermochemical process. *J. Soils Sediments* **2012**, *12* (8), 1211–1221; DOI: 10.1007/s11368-
411 012-0489-x.
- 412 11. Warnock, D. D.; Lehmann, J.; Kuyper, T. W.; Rilling, M. C. Mycorrhizal responses to
413 biochar in soil – concepts and mechanisms. *Plant Soil* **2007**, *300* (1-2), 9-20; DOI:
414 10.1007/s11104-007-9391-5.
- 415 12. Liang, B.; Lehmann, J.; Solomon, D.; Kinyangi, J.; Grossman, J.; O'Neill, B.; Skjemstad, J.
416 O.; Thies, J.; Luizão, F. J.; Petersen, J.; Neves, E. G. Black Carbon Increases Cation
417 Exchange Capacity in Soils. *Soil Sci. Soc. Am. J.* **2006**, *70* (5), 1719-1730;
418 DOI:10.2136/sssaj2005.0383.
- 419 13. Thomas, S. C.; Frye, S.; Gale, N.; Garmon, M.; Launchbury, R.; Machado, N.; Melamed, S.;
420 Murray, J.; Petroff, A.; Winsborough, C. Biochar mitigates negative effects of salt additions

- 421 on two herbaceous plant species. *J. Environ. Manage.* **2013**, *129*, 62–68; DOI:
422 10.1016/j.jenvman.2013.05.057.
- 423 14. Chan, K. Y.; Van Zwieten, L.; Meszaros, I.; Downie, A.; Joseph, S. Agronomic values of
424 greenwaste biochar as a soil amendment. *Soil Res.* **2007**, *45* (8), 629–634; DOI:
425 10.1071/SR07109.
- 426 15. Steinbeiss, S.; Gleixner, G.; Antonietti, M. Effect of biochar amendment on soil carbon
427 balance and soil microbial activity. *Soil Biol. Biochem.* **2009**, *41* (6), 1301–1310; DOI:
428 10.1016/j.soilbio.2009.03.016.
- 429 16. Novak, J. M.; Busscher, W. J.; Laird, D. L.; Ahmedna, M.; Watts, D. W.; Niandou, M. A. S.
430 Impact of Biochar Amendment on Fertility of a Southeastern Coastal Plain Soil. *Soil Sci.*
431 **2009**, *174* (2), 105-112; DOI: 10.1097/SS.0b013e3181981d9a.
- 432 17. Zimmerman, A. R.; Gao, B.; Ahn, M.-Y. Positive and negative carbon mineralization
433 priming effects among a variety of biochar-amended soils. *Soil Biol. Biochem.* **2011**, *43* (6),
434 1169-1179; DOI: 10.1016/j.soilbio.2011.02.005.
- 435 18. McClellan, T.; Deenik, J.; Uehara, G.; Antal, M. Effects of flashed carbonized macadamia
436 nutshell charcoal on plant growth and soil chemical properties. *Am. Chem. Soc. Agron.*
437 *Abstr.* **2007**.
- 438 19. McLaughlin, H.; Anderson, P. S.; Shields F. E.; Reed, T. B. All biochars are not created
439 equal, and how to tell them apart. *Proceedings, North American Biochar Conference,*
440 *Boulder, Colorado, 2009*, [www.biochar-international.org/sites/default/files/All-Biochars--](http://www.biochar-international.org/sites/default/files/All-Biochars--Version2--Oct2009.pdf)
441 [Version2--Oct2009.pdf](http://www.biochar-international.org/sites/default/files/All-Biochars--Version2--Oct2009.pdf)
- 442 20. McBeath, A. V.; Smernik, R. J. Variation in the degree of aromatic condensation of chars.
443 *Org. Geochem.* **2009**, *40* (12), 1161-1168; DOI: 10.1016/j.orggeochem.2009.09.006.
- 444 21. Cao, X.; Harris, W. Properties of dairy-manure-derived biochar pertinent to its potential use
445 in remediation. *Bioresource Technol.* **2010**, *101* (14), 5222-5228;
446 DOI: 10.1016/j.biortech.2010.02.052.

- 447 22. Knicker, H. Pyrogenic organic matter in soil: its origin and occurrence, its chemistry and
448 survival in soil environments. *Quatern, Int.* **2011**, *243* (2), 251-263; DOI:
449 10.1016/j.quaint.2011.02.037.
- 450 23. Schimmelpfennig, S.; Glaser, B. One step forward toward characterization: Some important
451 material properties to distinguish biochars. *J. Environ. Quality* **2012**, *41*, 1001-1013; DOI:
452 10.2134/jeq2011.0146.
- 453 24. Wiedner, K.; Naisse, C.; Rumpel, C.; Pozzi, A.; Wieczorek, P.; Glaser, B. Chemical
454 modification of biomass residues during hydrothermal carbonization – What makes the
455 difference, temperature or feedstock? *Org. Geochem.* **2013**, *54*, 91-100; DOI:
456 10.1016/j.orggeochem.2012.10.006.
- 457 25. Zhao, L.; Cao, X.; Mašek, O.; Zimmerman, A. Heterogeneity of biochar properties as a
458 function of feedstock sources and production temperatures. *J. Hazard. Mater.* **2013**, *256*-
459 *257*, 1-9; DOI:10.1016/j.jhazmat.2013.04.015.
- 460 26. Conte, P.; Marsala, V.; De Pasquale, C.; Bubici, S.; Valagussa, M.; Pozzi, A.; Alonzo, G.
461 Nature of water-biochar interface interactions. *GCB Bioenergy* **2013**, *5* (2), 116–121; DOI:
462 10.1111/gcbb.12009.
- 463 27. Sing, K. The use of nitrogen adsorption for the characterization of porous materials. *Colloid.*
464 *Surface. A.* **2001**, *187-188*, 3-9; DOI: 10.1016/S0927-7757(01)00612-4.
- 465 28. Dunn, K. J.; Bergman D. J.; Latorraca G. A. *Handbook of geographic exploration-seismic*
466 *exploration: Nuclear Magnetic Resonance Petrophysical and Logging Applications*;
467 Elsevier Science Ltd: Oxford, U.K., 2002.
- 468 29. Conte, P.; Alonzo, G. Environmental NMR: Fast-field-cycling Relaxometry, *eMagRes*,
469 **2013**, 389–398; DOI 10.1002/9780470034590.emrstm1330.
- 470 30. Kimmich, R.; Anardo, E. Field-cycling NMR relaxometry. *Prog. Nucl. Mag. Res. Sp.*
471 **2004**, *44*, 257–320; DOI: 10.1016/j.pnmrs.2004.03.002.

- 472 31. Morozova-Roche, L. A.; Jones, J. A.; Noppe, W.; Dobson, C. M. Independent Nucleation
473 and Heterogeneous Assembly of Structure during Folding of Equine Lysozyme. *J. Mol.*
474 *Biol.* **1999**, *289* (4), 1055-1073; DOI: 10.1006/jmbi.1999.2741.
- 475 32. Borgia, G. C.; Brown, R. J. S.; Fantazzini, P. Uniform-Penalty Inversion of
476 Multiexponential Decay Data. *J. Magn. Reson.* **1998**, *132* (1), 65-77; DOI:
477 10.1006/jmre.1998.1387.
- 478 33. Borgia, G. C.; Brown R. J. S.; Fantazzini, P. Uniform-Penalty Inversion of Multiexponential
479 Decay Data: II. Data Spacing, T_2 Data, Systematic Data Errors, and Diagnostics. *J. Magn.*
480 *Reson.* **2000**, *147* (2), 273-285; DOI: 10.1006/jmre.2000.2197.
- 481 34. Almendros, G.; Martinez, A. T.; Gonzalez, A. E.; Gonzalez-Vila F. J.; Freund, R.;
482 Luedemann, H.-D. CPMAS ^{13}C NMR study of lignin preparations from wheat straw
483 transformed by five lignocellulose-degrading fungi. *J. Agric. Food Chem.* **1992**, *40* (7),
484 1297-1302; DOI: 10.1021/jf00019a043.
- 485 35. Callaghan, P. T.; Coy, A. PGSE NMR and molecular translational motion in porous media.
486 In *Nuclear magnetic resonance probes of molecular dynamics*; Tycho, R., Ed.; Kluwer
487 Academic Publishers: Dordrecht NL 1994; pp. 551.
- 488 36. Godward, J.; Gunning, P.; Hills, B.P. An NMR protocol for determining ice crystal size
489 distributions during freezing and pore size distributions during freeze-drying. *Appl. Magn.*
490 *Reson.* **1999**, *17* (4), 537-556; DOI: 10.1007/BF03162085.
- 491 37. Brownstein, K. R.; Tarr, C. E. Importance of classical diffusion in NMR studies of water in
492 biological cells. *Phys. Rev. A* **1979**, *19* (6), 2446-2454; DOI: 10.1103/PhysRevA.19.2446.
- 493 38. Laudicina, V. A.; De Pasquale, C.; Conte, P.; Badalucco, L.; Alonzo, G.; Palazzolo, E.
494 Effects of afforestation with four unmixed plant species on the soil–water interactions in a
495 semiarid Mediterranean region (Sicily, Italy). *J. Soil Sediment* **2012**, *12* (8), 1222–1230;
496 DOI 10.1007/s11368-012-0522-0.

- 497 39. Stingaciu, L. R.; Pohlmeier, A.; Blümmler, P.; Weihermüller, L.; van Dusschoten, D.; Stapf,
498 S.; Vereecken, H. Characterization of unsaturated porous media by high-field and low-field
499 NMR relaxometry, *Water Resour. Res.* **2009**, *45* (8), DOI:10.1029/2008WR007459.
- 500 40. Korb, J.-P. Surface diffusion of liquids in disordered nanopores and materials: a field
501 cycling relaxometry approach. In *Fluid transport in nanoporous materials*; Conner W. C.;
502 Fraissard J., Eds.; Academic Press: Springer, NL, 2006.
- 503 41. Bakhmutov, V. I. Front Matter. In *Practical NMR relaxation for chemists*; John Wiley &
504 Sons, Ltd: Chichester, U.K., 2004.
- 505

506 **Figure captions**

507 **Figure 1.** CP-TOSS ^{13}C NMR spectra of poplar hydrochar (**A**) and pyrochar (**B**)

508 **Figure 2.** Relaxograms of poplar hydrochar (**A**) and pyrochar (**B**) acquired at the proton

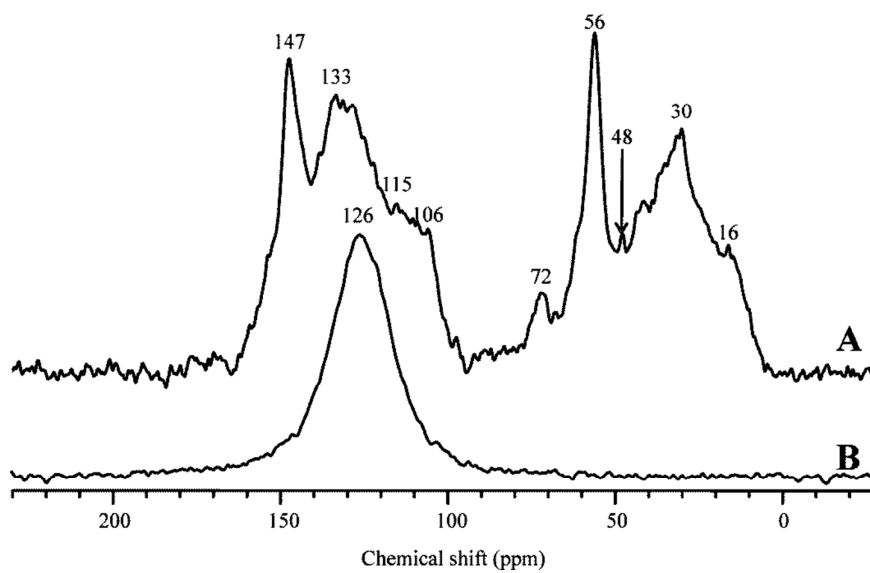
509 Larmor frequency of 40 MHz

510 **Figure 3.** NMRD profiles of poplar hydrochar (**A**) and pyrochar (**B**)

511

512

513



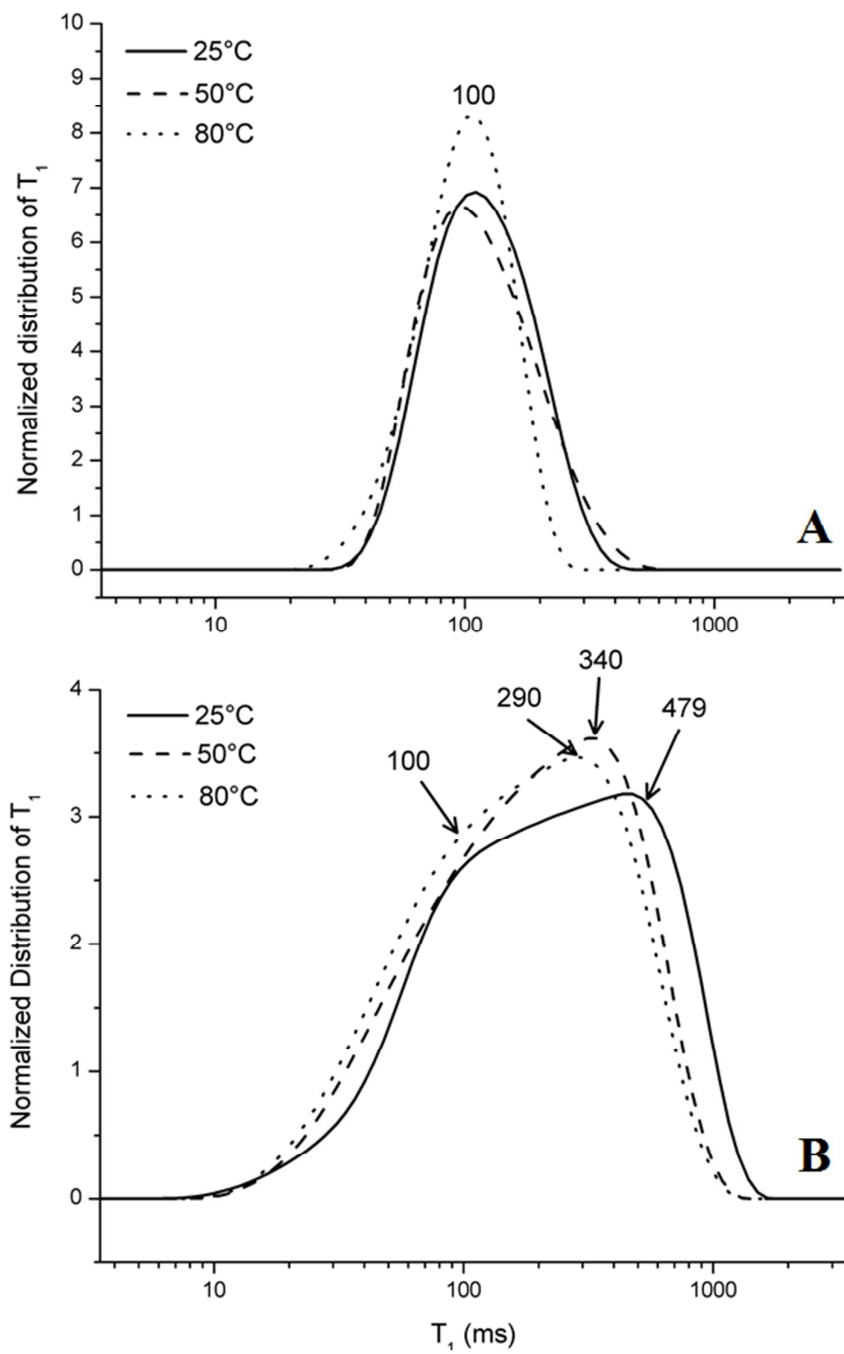
514

515

516

517

Figure 1



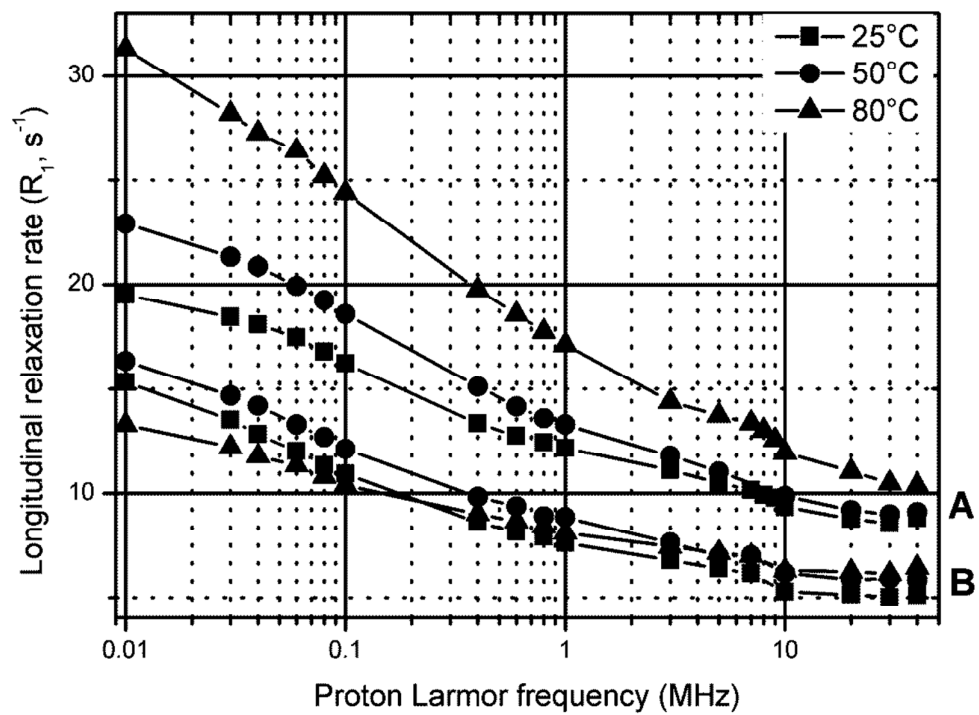
518

519

520

Figure 2

521



522

523

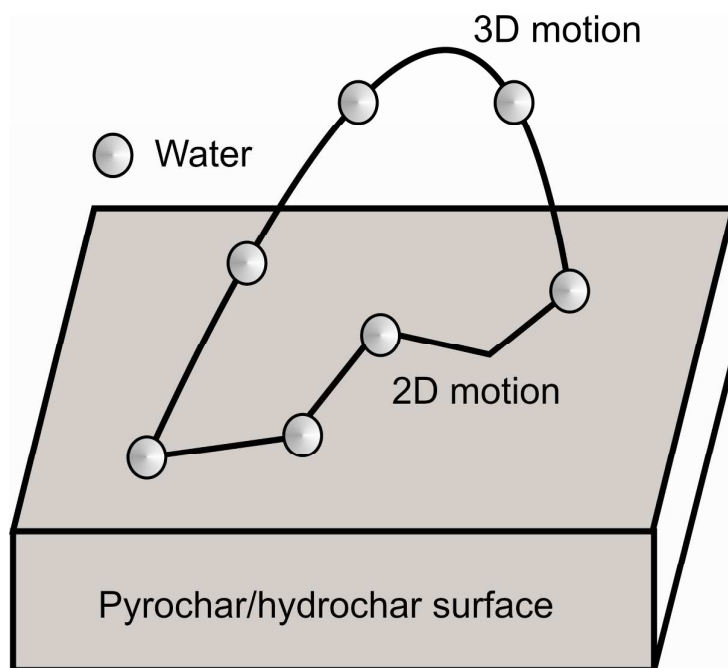
Figure 3

524

525

Table of Contents/Abstract Graphic

526



527